ACS APPLIED MATERIALS & INTERFACES

Research Article

www.acsami.org

A Rapid, Solvent-Free Protocol for the Synthesis of Germanium Nanowire Lithium-Ion Anodes with a Long Cycle Life and High Rate Capability

Emma Mullane,[§] Tadhg Kennedy,[§] Hugh Geaney, and Kevin M. Ryan*

Materials and Surface Science Institute and the Department of Chemical and Environmental Sciences, University of Limerick, Limerick, Ireland

Supporting Information

ABSTRACT: A rapid synthetic protocol for the formation of high-performance Ge nanowire-based Li-ion battery anodes is reported. The nanowires are formed in high density by the solvent-free liquid deposition of a Ge precursor directly onto a heated stainless steel substrate under inert conditions. The novel growth system exploits the in situ formation of discrete Cu_3Ge catalyst seeds from 1 nm thermally evaporated Cu layers. As the nanowires were grown from a suitable current collector, the electrodes could be used directly without binders in lithium-ion half cells. Electrochemical testing showed remarkable capacity retention with 866 mAh/g achieved after 1900 charge/discharge cycles and a Coulombic efficiency of 99.7%. The nanowire-based anodes also showed high-rate stability with discharge capacities of 800 mAh/g when cycled at a rate of 10C.

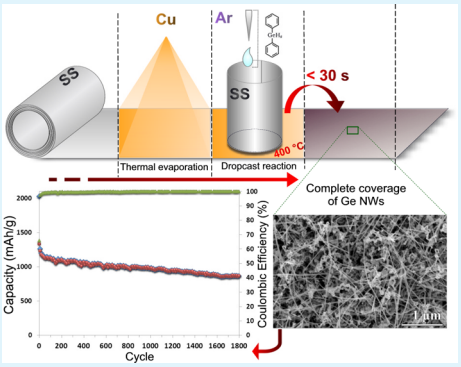

KEYWORDS: *germanium nanowires, lithium-ion battery, high capacity, long cycle life, porous, network*

INTRODUCTION

The ever-increasing power demands of mobile technologies and, in particular, the requirements of electric vehicles in terms of range and cost, needs Li-ion batteries with significantly increased energy densities. For this to be realized, major material advances are needed with technologies that are suitably scalable, cost-effective, and have minimal environmental impact.[1−3] The anode component of current commercial Li-ion batteries is typically composed of graphite (theoretical capacity of 372 mAh/g); however, Ge and Si boast multiples of this due their ability to form lithium-rich alloys. The formation of the lithiated alloys $Li_{15}Ge_4$ (1384 mAh/g) and $Li_{15}Si_4$ (3579 mAh/g) leads to considerable expansion of bulk Ge and Si (>300%), which causes pulverisation of the material, ultimately limiting the cycle life of Li-alloying anodes.[4−8] Ge and Si nanowires (NWs) offer potential for circumventing this issue by accommodating this volume expansion through a crystalline to amorphous phase transition while retaining structural integrity.[9−16] The anchoring of the NWs directly to the substrate also allows for elimination of binders that further reduces the overall weight of the battery and increases the energy density.[4,5] A challenge is that the radial expansion of the NWs on lithiation can progressively lead to cleavage from the current collector. This is usually apparent from a continuously diminishing capacity through extended cycling. Innovative approaches to tuning the expansion through constraining the NWs in core−shell morphologies can allow extended cycling with extremely high capacities.[2,16,17] The additional synthetic steps for such compositions, however, may mitigate against scalable formation mechanisms for large-scale production. We recently have shown the exemplary stability of Ge NW-based anodes that are produced in a long-necked round-bottom flask using the vapor phase of a high boiling point solvent as the growth zone.[11,18] An advantage of this process is the in situ formation of Sn nanoparticles from a thermally evaporated layer, thereby eliminating the separate synthetic steps that are intensive to form size-controlled mondisperse seeds.[10] Integral to the long cycle life (>1000 cycles) is the transformation of this dense NW array into a continuous porous network in the first 100 cycles that completely eliminates cycle losses thereafter. While the NWs perform exceptionally well as a Li-ion anode material, a potential barrier to the industrial application of this synthesis method is the batch nature of the glassware approach that would limit the large area formation of NWs for scalable production. The more conventional route to Ge NW synthesis is that of chemical vapor deposition (CVD), but this also has the disadvantage of being a high-cost technique requiring highly specialized equipment. If Ge NW electrodes are to become a viable alternative to current graphitic-based Li-ion anodes, it is essential that more simplified, cost-effective, and rapid NW synthesis methods are developed that may ideally be compatible with current industrial techniques, for example, a roll to roll process.

Received: July 11, 2014
Accepted: October 21, 2014
Published: October 21, 2014

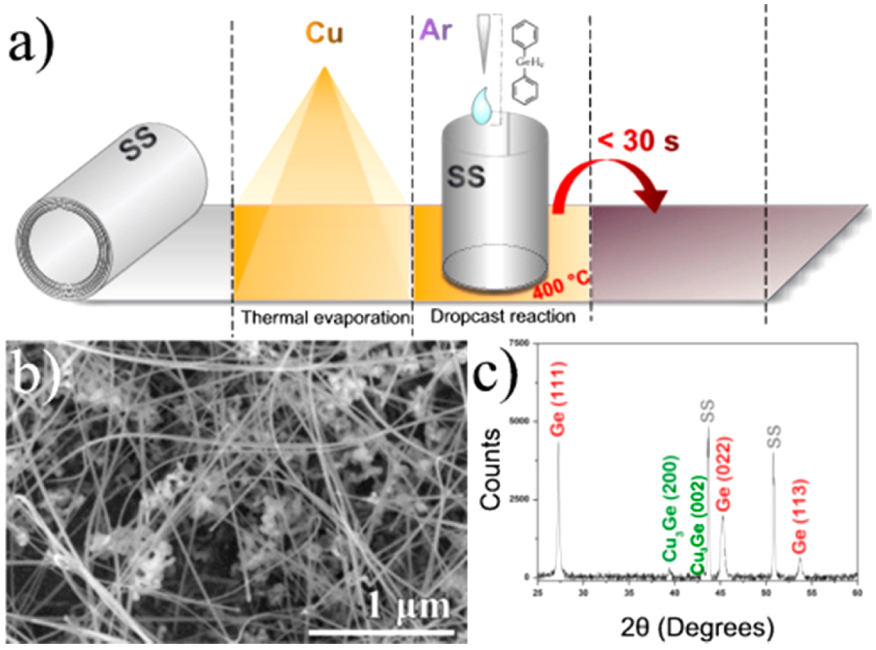

Figure 1. (a) Schematic of the growth system that allows dense Ge NW growth on cm^2 substrates. (b) SEM image of NWs grown directly from the SS current collector showing a mixture of straight and tortuous NWs. (c) XRD analysis of the NW-covered substrate showing reflections consistent with the presence of Ge NWs, SS current collector, and low-intensity reflections from the Cu_3Ge catalyst seeds.

In this report we develop a new and rapid synthetic protocol for the formation of Ge NW-based Li-ion anodes using Cu on stainless steel (SS) as the growth substrate. Using a very simple reaction protocol, NW growth occurs in less than 30 s by thermolytic decomposition of an organometallic precursor (diphenylgermane (DPG)) onto a preheated substrate in an inert atmosphere. NW catalysis occurs via a vapor−solid−solid (VSS) growth mechanism[18−23] and exploits the propensity of thin Cu layers (≤10 nm) to form discrete Cu_3Ge nanoparticle seeds when heated in contact with Ge monomer.[24−26] The formation of solid catalyst seeds in situ is advantageous as it facilitates uniform growth of NWs across the current collector surface while also limiting agglomeration, which can impact preformed catalyst seeds. The solvent-free method allows for the formation of dense, well-anchored Ge NW layers on centimeter-scale substrates, which can be directly integrated as Li-ion battery anodes. The use of a 1 nm Cu catalyst layer allows robust anchoring of the NWs to the current collector while also ensuring that the amount of inactive material on the anode is kept to an absolute minimum (no binders or conductive additives are required). Electrochemical analysis of the NW-covered substrates show exceptional performance with capacities of 866 mAh/g after 1900 charge/discharge cycles. Importantly, the density of the NWs obtained by this approach also allows for their transformation into a continuous porous network that is the optimal architecture for stable cycling. The facile synthesis method exhibits considerable promise as a rapid, solvent-free, high throughput approach to the formation of next-generation Li-ion battery anodes.

EXPERIMENTAL SECTION

Substrate Preparation and Post-Synthetic Treatment. Stainless steel (SS, 316) foil was purchased from Pi-Kem Ltd. with a thickness of 0.1 mm and was untreated prior to use. Cu (99.999% Kurt J. Lesker) was thermally evaporated onto the SS substrates in a glovebox-based evaporation unit. After the growth reactions, the NW-covered substrates were removed from the glovebox for analysis.

Chemicals Used. All chemicals were used as received. Diphenylgermane (DPG) (97%) was supplied by Gelest and was stored and dispensed from an Ar-filled glovebox.

Reaction Setup. Reactions were carried out in an Ar-filled glovebox using a Stuart CD162 digital stirrer/hot plate with a maximum temperature of 450 °C. Substrates for the reaction were placed on the hot plate at 425 °C, and the temperature was allowed to equilibrate for 1 min prior to reaction. The SS "confiner" was placed on to the SS substrate just before reaction. The appropriate volume (10 μL) of the precursor was then drop-cast onto the substrate. The droplet was allowed to evaporate, thus terminating the reaction, and the substrate was removed from the hot plate for analysis.

Analysis. Scanning electron microscopy (SEM) analysis was performed on a Hitachi SU-70 system operating between 3 and 20 kV. For transmission electron microscopy (TEM) analysis, the NWs were removed from the substrates through the use of a sonic bath. TEM analysis was conducted using a 200 kV JEOL JEM-2100F field emission microscope equipped with a Gatan Ultrascan CCD camera and EDAX Genesis EDS detector. XRD analysis was conducted using a PANalytical X'Pert PRO MRD instrument with a Cu Kα radiation source (λ = 1.5418 Å) and an X'celerator detector. The mass of the Ge NWs per electrode was determined through careful measurement using a Sartorius Ultra-Microbalance SE2 (repeatability ±0.25 μg).

Electrochemical Measurements. The electrochemical performance was evaluated by assembling two electrode Swagelok type cells in an Ar-filled glovebox. The cells consisted of the as-synthesized Cu_3Ge-seeded Ge NWs on SS substrates as the working electrode, Li foil as the counter and reference electrodes, a porous polypropylene Celgard separator, and an electrolyte solution of 1 M $LiPF_6$ in ethylene carbonate/dimethyl carbonate (EC/DMC) (1:1 v/v) + 3 wt % vinylene carbonate (VC). The cycling measurements were carried out galvanostatically using a Biologic MPG-2 multichannel potentiostat in the potential range of 0.01−1.5 V versus Li/Li^+. The cyclic voltammetry experiment was carried out in the potential range of 0.01−2.0 V at a scan rate of 1 mV s^{-1} also on the Biologic MPG-2.

RESULTS AND DISCUSSION

The novel synthetic protocol developed for Ge NW growth is depicted schematically in Figure 1a. The simple process involves a Cu-coated SS substrate with Ge NW growth

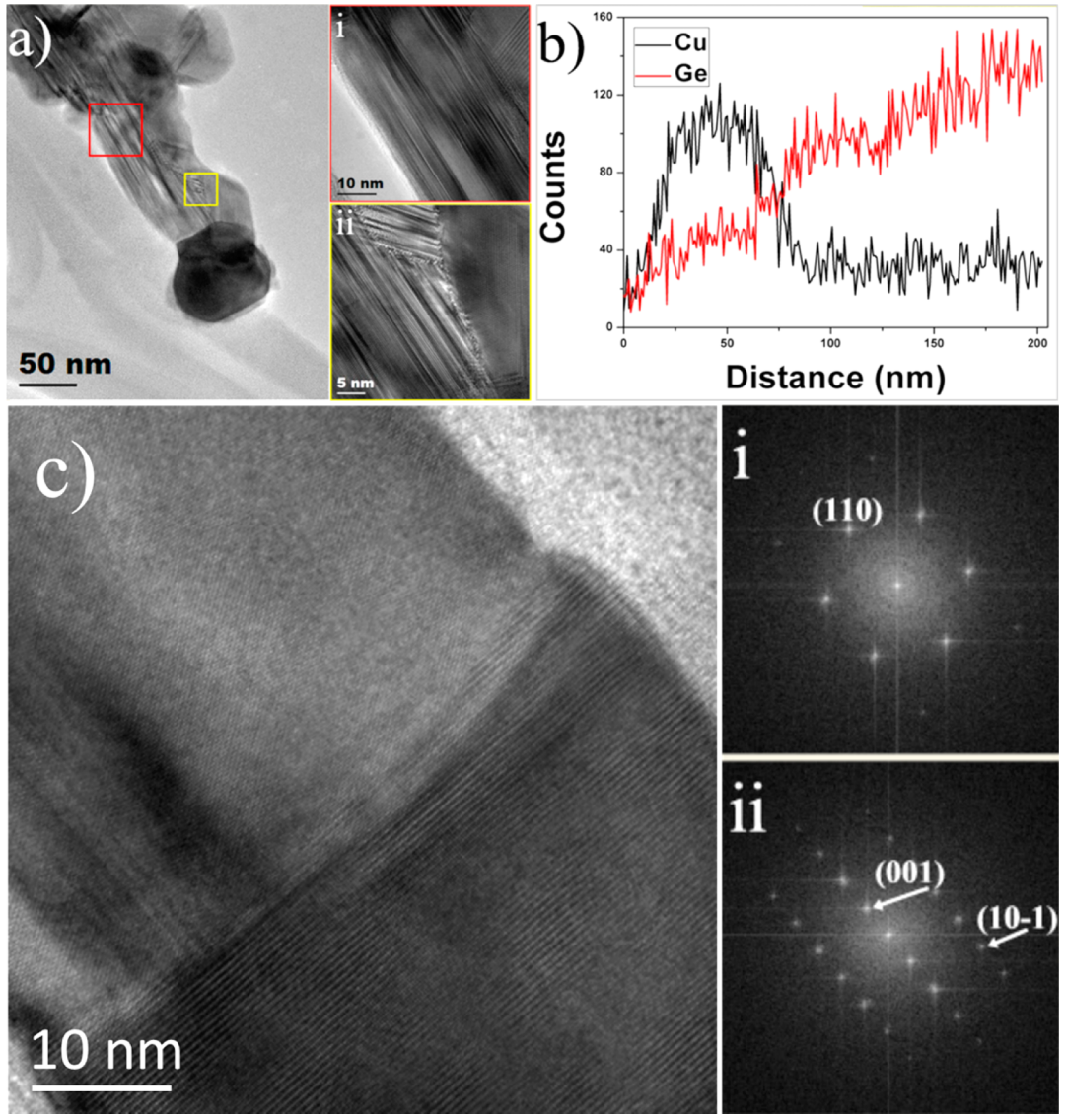

Figure 2. (a) Bright-field TEM image of a wormlike Cu_3Ge-seeded Ge NW illustrating the high defect density (insets (i) and (ii)). (b) Energy-dispersive X-ray line profile collected from a Cu_3Ge-seeded NW. (c) High-resolution TEM image of straight Ge NW with inset FFTs (i) and (ii) corresponding to the crystalline Ge NW and Cu_3Ge seed, respectively.

initiated by drop casting a liquid precursor solution, namely, DPG, directly onto the heated substrate in an inert atmosphere. To ensure conformal NW growth, an inert SS confiner is used to confine the liquid droplet to localize growth. When heated, the thin Cu layer on the substrate forms discrete nanoparticles, which are converted to Cu_3Ge seeds when in contact with Ge monomer from the thermally decomposed DPG precursor. Ge NW growth then ensues via a VSS growth mechanism, with the reaction terminating once the precursor droplet has evaporated (<30 s). (See Supporting Information Figure S1 for photographic images of a pre- and post-reaction substrate.) These reaction times are sufficient to allow dense NW coverage on the SS substrate that is comparable with our previous reports that used a solvent vapor growth (SVG) regime.[27−29] The major advance of this new system is the short electrode fabrication time (<2 min) as opposed to the SVG protocol where typical reactions take up to 2 h in total (encompassing solvent degassing, temperature ramping, reaction time, and cooling). The short processing times allow for high throughput, which is ultimately attractive from an industrial viewpoint.

Despite the marked difference in processing times, the rapid method is also suitable for the formation of high aspect-ratio NWs. Post-synthetic SEM analysis (Figure 1b) shows the formation of a mixture of straight and wormlike NWs directly from the substrate. The XRD diffractogram shown in Figure 1c shows reflections that are consistent with the (111), (022), and (113) spacings for cubic Ge with space group $Fd\bar{3}m$. The underlying SS substrate reflections are also indexed along with the (200) and (002) reflections from Cu_3Ge. It was found there is a direct correlation between the thickness of the as-deposited Cu film and the size of the seeds obtained. For a 1 nm Cu layer, catalytic particles of roughly 10−30 nm (Supporting Information, Figure S2) formed, while 10 nm initial layer thickness led to the formation of >100 nm particles (Supporting Information, Figure S3). In contrast, 20 nm Cu layers produced a solid Cu_3Ge layer (Supporting Information, Figure S4) across the substrate surface prior to NW growth.

The NWs formed in this study can be categorized into two types: highly defected (wormlike) and straight single crystal. The TEM image of the wormlike NW (Figure 2a) clearly

shows the Cu_3Ge seed on the NW tip and also crystallographic defects that are visible even at low magnification. A high-resolution image taken from the highlighted areas in Figure 2a is shown in insets (i) and (ii). The defects in (i) can be seen to be a mixture of commonly noted longitudinal and transverse faults.[28,30,31] The portion of the NW shown in (ii) has a defect-free region framed by multiple defects. Energy-dispersive X-ray spectroscopy (EDX) line analysis was performed on a single NW shown in Figure 2b. The region that shows a high Cu signal and nonzero Ge signal corresponds to the Cu_3Ge seed with the NW composed solely of Ge. High-resolution TEM analysis of a typical straight NW in Figure 2c illustrates the ⟨110⟩ growth direction typically seen for Cu_3Ge-seeded NWs. The fast Fourier transforms (FFTs) (insets (i) and (ii)) are indexed for cubic Ge and orthorhombic Cu_3Ge, respectively.

To test the performance of the Ge NWs as a Li-ion anode material, Ge NW electrodes were synthesized from a 1 nm thick Cu layer on SS. The extremely thin layer ensures that each individual NW is directly contacted to the current collector. The electrochemical performance was tested by galvanostatic cycling experiments, which were carried out using two electrode Swagelok cells. The as-grown Ge NWs from SS were used directly as the working electrode and were cycled versus lithium ribbon, which acted as both the counter and reference electrode. The NWs were cycled at a 1C rate in the voltage range of 0.01−1.5 V in a 1 M $LiPF_6$ in EC/DMC (1:1 v/v) + 3 wt % VC electrolyte with the results shown in Figure 3a and voltage profiles in Figure 3b. The electrodes had a loading density of 0.19 mg of active material per cm^2, and the average thickness of active material was between 1.5−2.0 μm. The NWs exhibited an impressive initial discharge capacity of 1333 mAh/g, 96% of the maximum achievable theoretically. The capacity retention of the electrode was excellent, retaining a capacity of 866 mAh/g after 1900 cycles, well over twice the maximum achievable of conventional graphitic-based anodes. Inspection of the data reveals that there is a gradual decline in the capacity over the first 50 cycles, fading from 1333 to 1128 mAh/g. From 50 cycles onward, the performance of the electrode stabilized, retaining 76% of its capacity for the following 1850 cycles and exhibiting an impressive average Coulombic efficiency (C.E.) of 99.7%.

To investigate the contribution of the Cu_3Ge seeds to the overall capacity, an electrode was fabricated using the same procedure as before but limiting the reaction temperature to 375 °C, below the minimum temperature required for NW growth. This ensured that the 1 nm Cu layer was converted to Cu_3Ge particles, yet no Ge NW growth occurred. When galvanostatically cycled versus Li metal at a rate of 100 mA/g, the Cu_3Ge electrode exhibited a capacity of 19 mAh/g after 150 cycles (Supporting Information, Figure S5). As the mass of the Cu_3Ge seeds in the Ge NW electrodes is only ∼1% of the total mass of active material, the contribution of the seeds to the overall capacity is deemed to be negligible.

As stated previously the use of an initial 1 nm catalytic Cu layer ensures that each NW is directly anchored to the SS current collector, a property that is a prerequisite for stable capacity retention. When using a thicker thermally evaporated catalytic Cu layer (>10 nm), the NW growth mechanism proceeds via the initial formation of a continuous Cu_3Ge layer (as opposed to discrete nanoparticles) on the substrate followed by NW growth from this film as noted previously by Geaney et al.[19] While dense NW growth from thicker Cu layers is also obtained (Supporting Information, Figure S6), the

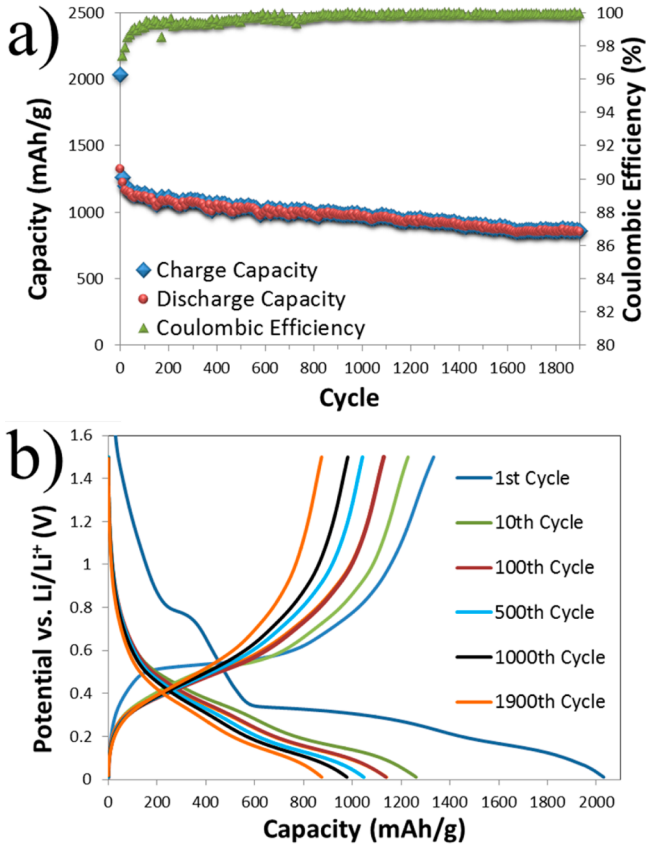

Figure 3. (a) Charge capacity (blue markers), discharge capacity (red markers), and Coulombic efficiencies (green markers) of a Ge NW electrode synthesized using a 1 nm catalytic Cu layer. The electrodes were cycled at a 1C rate in the potential range of 0.01−1.5 V. (b) Voltage profiles of cycles 1, 10, 100, 500, 1000, and 1900 cycles. The profiles show characteristic plateaus corresponding to the lithiation and delithiation Ge.

underlying Cu_3Ge film readily cleaves from the metal substrate impeding their use in binder-free electrodes (Supporting Information, Figure S7). Typically, the anodes containing this continuous catalytic layer supporting the NWs show good capacity retention up to 50 cycles (Supporting Information, Figure S8), but there is a significant dropoff in capacity on continued cycling. This drop in performance can be attributed to the already partially delaminated/fractured film losing contact with the current collector on extended cycling as expected. The use of a catalyst layer of thickness ≤10 nm is thus optimal as it allows the formation of discrete Cu_3Ge catalyst particles, which allow direct connection between the individually anchored NWs and the SS electrode.

The superior capacity retention of the electrode synthesized using the 1 nm Cu layer is a direct result of the Ge NWs transforming into a mechanically robust, porous, stable network of Ge ligaments through cycling. We previously demonstrated this transformation process in a study of Sn-seeded Ge NWs, and evidence of the same phenomenon is apparent here.[11] Figure 4a,b shows a low-magnification tilted SEM image and a low-magnification TEM image of the active material after 50 cycles. The NWs have lost their wirelike morphology and have transformed into a spongelike system of Ge ligaments that remains well-contacted to the current collector. Higher magnification TEM and dark field scanning TEM (DFSTEM) images (Figure 4c,d) show the system of ligaments in more

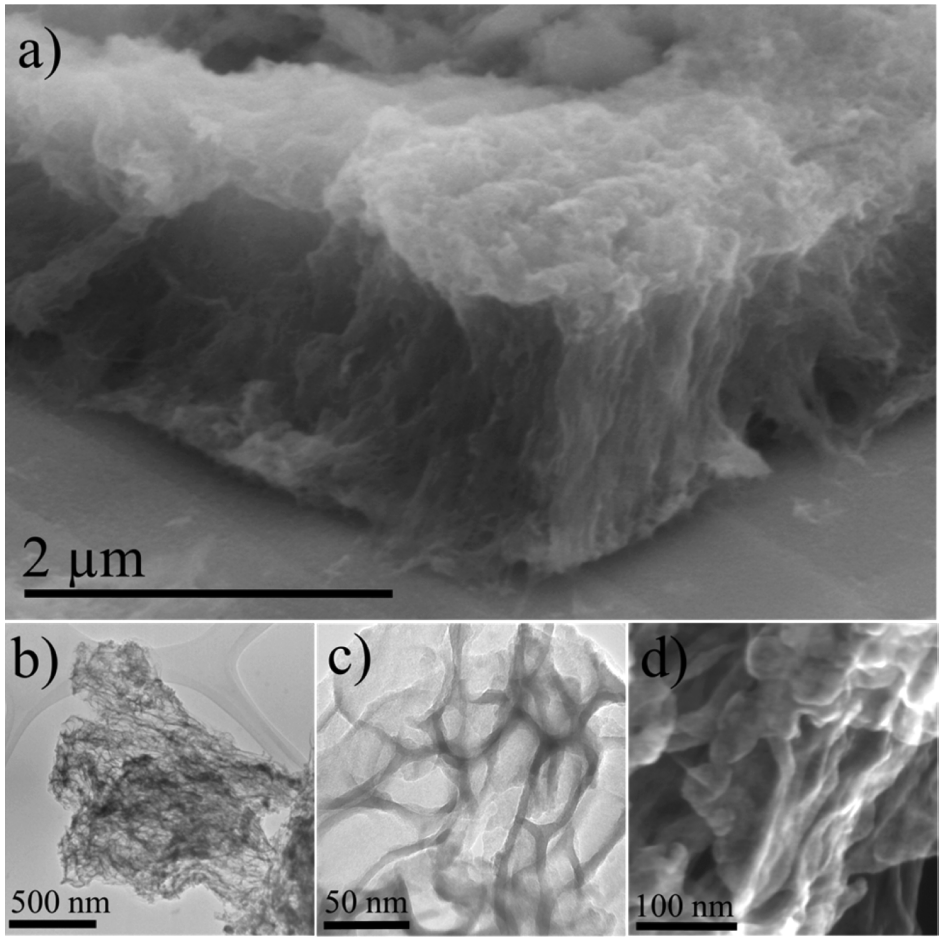

Figure 4. (a) SEM image of the active material after 50 charge−discharge cycles. The original NW morphology is lost having been replaced by a spongelike network of active material. (b) Low-magnification TEM image of the network architecture formed after 50 cycles. (c) Higher magnification TEM image of the active material after 50 cycles. The network is comprised of a series of interweaving ligaments of Ge. (d) Higher magnification DFSTEM image of the active material after 50 cycles.

detail. The convoluted nature of the transformed active material is evident with the individual ligaments interweaving and intertwining with one another. This effect is observed across the entire substrate, creating a continuous, porous network of active material. This porous construct has a profound effect on the performance of the anode material as the empty space can accommodate the volume changes without further capacity losses. Furthermore, the Ge ligaments of the network reach a critical diameter (~5.5 nm) below which no further deformation occurs due to cycling, explaining the excellent capacity retention of the electrode. This is evidenced by the fact that the morphology of the active material after 200 cycles (Supporting Information, Figure S9) is identical to that after 50 cycles, indicating the mechanical robustness of the network once it is formed.

To investigate the electrochemical processes occurring within the electrode during charging and discharging, the differential capacity was plotted at various stages of cycling (Figure 5a,b). A broad peak occurs between 0.7−0.9 V during the first charging cycle (Figure 5a), which does not reappear, and is due to SEI formation. The sharp peak at 0.33 V is due to the lithiation of c-Ge and also occurs only in the first cycle indicating that the NWs have become completely amorphous upon delithiation. For the remaining cycles broad peaks occur during charging at 0.47, 0.35, and 0.15 V and are due to the progressive lithiation of the active material to form a series of more Li-rich Li−Ge alloys (Ge → a-Li_xGe → a-$Li_{15}Ge_4$ → c-$Li_{15}Ge_4$).[32−35] During discharging a sharp peak is evident at 0.5 V and is due to the delithiation of the c-$Li_{15}Ge_4$ phase. As cycling progresses, this sharp peak decreases indicating that less of the crystalline alloy is being formed. Concomitantly, a broad peak emerges above 0.25 V due to the delithiation of the a-$Li_{15}Ge_4$ phase. By the 50th cycle the sharp peak at 0.5 V is all but gone, replaced by a broad peak between 0.25 and 0.85 V. Similar results were obtained from a cyclic voltammetry experiment wherein the onset of delithiation occurs at lower potentials with increasing cycle number (Figure 5c). Clearly these results indicate that as the active material transforms from the ordered NW structure to the more disordered porous network, the formation of the fully lithiated c-$Li_{15}Ge_4$ phase becomes less likely, and so the most Li-rich alloy formed during charging is the a-$Li_{15}Ge_4$ phase. This also explains the quicker decrease in capacity over the first 50 cycles compared with the rest of the data as less and less of the highest capacity and most Li-rich alloy, c-$Li_{15}Ge_4$, is being formed as cycling progresses. As the material becomes more disordered, progressively more of the fully lithiated active material exists as the lower capacity amorphous phase resulting in a steady drop for the first 50 cycles before the capacity stabilizes.

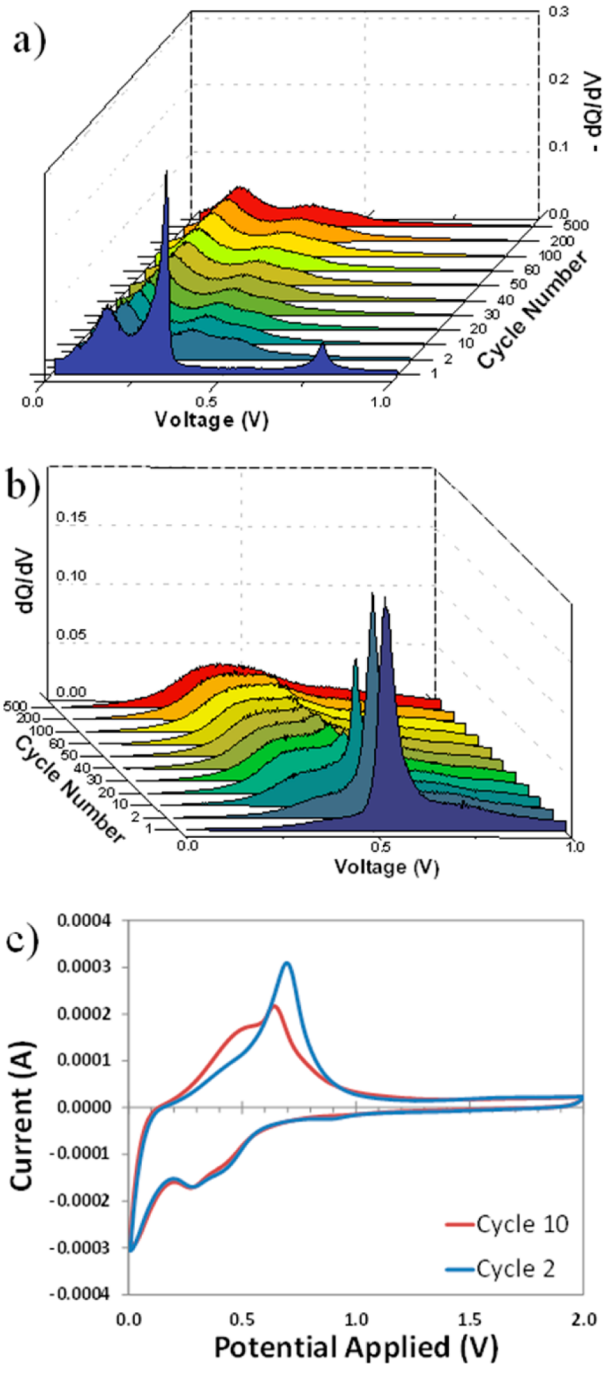

Figure 5. (a, b) Differential capacity plots taken from a range of cycles from 1 to 500 of a Ge NW electrode. The electrodes were cycled at a 1C rate in the potential range of 0.01−1.5 V. (a) The differential capacity of the charge sections is shown. (b) The differential capacity of the discharge sections is shown. The sharp peak at 0.5 V decreases in magnitude as cycling progresses indicating that increasingly less of the c-$Li_{15}Ge_4$ phase is formed upon full lithiation. (c) Cyclic voltammogram of the 2nd and 10th cycle of a Ge NW electrode. The experiment was performed at a scan rate of 1 mV/s in the voltage range of 0.01−2.0 V vs Li/Li^+. The shape of the delithiation section is very similar to that of the DCP in (b) with delithiation occurring at lower potentials for higher cycle numbers.

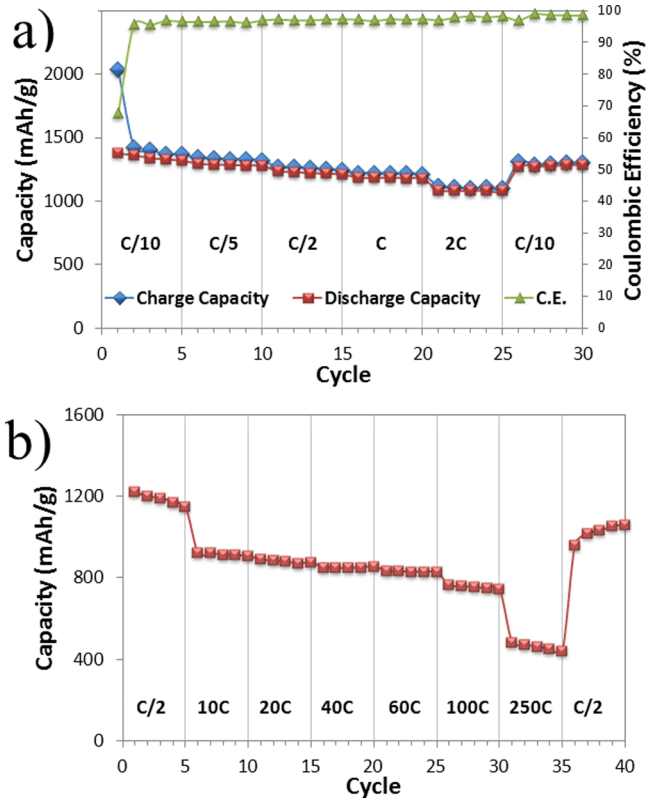

Figure 6. (a) Rate capability data of a Ge NW electrode charged and discharged in the voltage range of 0.01−1.5 V at rates of C/10, C/5, C/2, C, 2C, and then back to C/10. (b) High rate capability data of a Ge NW electrode. The discharge capacities measured for five cycles at seven different discharge rates are shown. The charge rate was kept constant at C/2 for all cycles. The electrode was charged and discharged in the voltage range of 0.01−1.5 V.

The rate capability of the Ge NW electrode was evaluated by charging and discharging the material for five cycles at rates of C/10, C/5, C/2, 1C, 2C, and then back to C/10 (Figure 6a). After five cycles at each rate the electrode exhibited discharge capacities of 1318, 1277, 1210, 1177, 1081, and 1285 mAh/g, respectively. Notably there was no significant abrupt drop in capacity observed when increasing the rate from C/10 as far as 1C. A slight drop of 90 mAh/g was noted when increasing the rate from 1C to 2C; however, when the rate was reduced back to C/10 the electrode retained 97.5% of its original capacity. The rate capability of the electrode at very high rates was also evaluated (Figure 6b). As the performance of Ge-based electrodes at very high rates is limited by the maximum achievable capacity during charging, the charge rate was kept constant at C/2 for all cycles while discharging at rates of C/2, 10C, 20C, 40C, 60C, 100C, 250C, and then back to C/2 (Figure 6b). The electrode performed very well maintaining discharge capacities of 1148, 908, 876, 857, 828, 745, and 439 mAh/g at each rate, respectively. The voltage profiles at each discharge rate and Coulombic efficiencies are presented in Supporting Information, Figure S10. The performance of the Ge NW electrode even at extremely high rates is jointly attributed to the high rate of diffusion of Li in Ge and the short diffusion distances provided by the nanostructured morphology. The rate capability of the electrodes suggests that the NWs may be suitable for high power applications designed to perform at very high discharge rates, such as electric vehicles and power tools.

dx.doi.org/10.1021/am5045168 | ACS Appl. Mater. Interfaces 2014, 6, 18800−18807

CONCLUSIONS

In conclusion, Cu_3Ge-seeded Ge NWs were successfully grown from SS current collectors through a low-energy pyrolysis route with reactions taking less than 30 s. The SS/NW array substrates could be directly incorporated into a lithium-ion half-cell for electrochemical testing. The thickness of the catalytic Cu layer was found to impact the capacity retention (over extended cycling) of the resultant NW-covered substrates with optimal results noted for a Cu layer thickness of 1 nm. Using this protocol the NW electrodes exhibited excellent capacity retention over 1900 cycles at a 1C rate, retaining a discharge capacity of 866 mAh/g. The electrode displayed excellent rate capability also maintaining a discharge capacity of 439 mAh/g even at the extremely high rate of 250C. The rapid pyrolysis route for the formation of active materials may be applied to other material sets and represents a rapid route for the formation of promising Li-ion battery anode materials.

ASSOCIATED CONTENT

Supporting Information

Additional information as described in the text. Images of pre- and post-reaction electrodes. SEM images of NWs grown from 1, 10, and 20 nm Cu layers. SEM and EDX analyses of Cu_3Ge layer synthesized from 20 nm layer of Cu. Charge capacity, discharge capacity, and Coulombic efficiencies of Cu_3Ge and of Ge NW electrode synthesized from 20 nm layer of Cu. TEM images of active material after 200 cycles. Voltage profiles of discharge portion of high rate capability test. This material is available free of charge via the Internet at http://pubs.acs.org.

AUTHOR INFORMATION

Corresponding Author

*E-mail: kevin.m.ryan@ul.ie.

Author Contributions

§Authors contributed equally.

Notes

The authors declare no competing financial interest.

ACKNOWLEDGMENTS

This work was supported by Science Foundation Ireland (SFI) under the Principal Investigator Program under Contract No. 11PI-1148 and also by EU FP7 funding—GREENLION Project—Contract No. 285268. T.K. acknowledges Intel Ireland and the Irish Research Council for funding through the Enterprise Partnership Scheme.

REFERENCES

(1) Osiak, M.; Geaney, H.; Armstrong, E.; O'Dwyer, C. Structuring Materials for Lithium-ion Batteries: Advancements in Nanomaterial Structure, Composition, and Defined Assembly on Cell Performance. *J. Mater. Chem. A* **2014**, *2*, 9433–9460.

(2) Arico, A. S.; Bruce, P.; Scrosati, B.; Tarascon, J.-M.; van Schalkwijk, W. Nanostructured Materials for Advanced Energy Conversion and Storage Devices. *Nat. Mater.* **2005**, *4*, 366–377.

(3) Liu, N.; Huo, K.; McDowell, M. T.; Zhao, J.; Cui, Y. Rice Husks as a Sustainable Source of Nanostructured Silicon for High Performance Li-ion Battery Anodes. *Sci. Rep.* **2013**, *3*, 1919.

(4) Chan, C. K.; Zhang, X. F.; Cui, Y. High Capacity Li-ion Battery Anodes Using Ge Nanowires. *Nano Lett.* **2007**, *8*, 307–309.

(5) Chan, C. K.; Peng, H.; Liu, G.; McIlwrath, K.; Zhang, X. F.; Huggins, R. A.; Cui, Y. High-Performance Lithium Battery Anodes using Silicon Nanowires. *Nat. Nanotechnol.* **2008**, *3*, 31–35.

(6) Chockla, A. M.; Bogart, T. D.; Hessel, C. M.; Klavetter, K. C.; Mullins, C. B.; Korgel, B. A. Influences of Gold, Binder and Electrolyte on Silicon Nanowire Performance in Li-Ion Batteries. *J. Phys. Chem. C* **2012**, *116*, 18079–18086.

(7) Chockla, A. M.; Klavetter, K.; Mullins, C. B.; Korgel, B. A. Tin-Seeded Silicon Nanowires for High Capacity Li-Ion Batteries. *Chem. Mater.* **2012**, *24*, 3738–3745.

(8) Chockla, A. M.; Klavetter, K. C.; Mullins, C. B.; Korgel, B. A. Solution-Grown Germanium Nanowire Anodes for Lithium-Ion Batteries. *ACS Appl. Mater. Interfaces* **2012**, *4*, 4658–4664.

(9) Yuan, F.-W.; Yang, H.-J.; Tuan, H.-Y. Alkanethiol-Passivated Ge Nanowires as High-Performance Anode Materials for Lithium-Ion Batteries: The Role of Chemical Surface Functionalization. *ACS Nano* **2012**, *6*, 9932–9942.

(10) Mullane, E.; Kennedy, T.; Geaney, H.; Dickinson, C.; Ryan, K. M. Synthesis of Tin Catalyzed Silicon and Germanium Nanowires in a Solvent–Vapor System and Optimization of the Seed/Nanowire Interface for Dual Lithium Cycling. *Chem. Mater.* **2013**, *25*, 1816–1822.

(11) Kennedy, T.; Mullane, E.; Geaney, H.; Osiak, M.; O'Dwyer, C.; Ryan, K. M. High-Performance Germanium Nanowire-Based Lithium-ion Battery Anodes Extending Over 1000 Cycles Through in Situ Formation of a Continuous Porous Network. *Nano Lett.* **2014**, *14*, 716–723.

(12) Chan, C. K.; Patel, R. N.; O' Connell, M. J.; Korgel, B. A.; Cui, Y. Solution-Grown Silicon Nanowires for Lithium-Ion Battery Anodes. *ACS Nano* **2010**, *4*, 1443–1450.

(13) Chan, C. K.; Ruffo, R.; Hong, S. S.; Huggins, R. A.; Cui, Y. Structural and Electrochemical Study of the Reaction of Lithium with Silicon Nanowires. *J. Power Sources* **2009**, *189*, 34–39.

(14) Chan, C. K.; Ruffo, R.; Hong, S. S.; Cui, Y. Surface Chemistry and Morphology of the Solid Electrolyte Interphase on Silicon Nanowire Lithium-ion Battery Anodes. *J. Power Sources* **2009**, *189*, 1132–1140.

(15) Chockla, A. M.; Harris, J. T.; Akhavan, V. A.; Bogart, T. D.; Holmberg, V. C.; Steinhagen, C.; Mullins, C. B.; Stevenson, K. J.; Korgel, B. A. Silicon Nanowire Fabric as a Lithium Ion Battery Electrode Material. *J. Am. Chem. Soc.* **2011**, *133*, 20914–20921.

(16) Choi, N.-S.; Yao, Y.; Cui, Y.; Cho, J. One Dimensional Si/Sn -Based Nanowires and Nanotubes for Lithium-ion Energy Storage Materials. *J. Mater. Chem.* **2011**, *21*, 9825–9840.

(17) Wu, H.; Chan, G.; Choi, J. W.; Ryu, I.; Yao, Y.; McDowell, M. T.; Lee, S. W.; Jackson, A.; Yang, Y.; Hu, L. Stable Cycling of Double-Walled Silicon Nanotube Battery Anodes Through Solid-Electrolyte Interphase Control. *Nat. Nanotechnol.* **2012**, *7*, 310–315.

(18) Geaney, H.; Mullane, E.; Ryan, K. M. Solution Phase Synthesis of Silicon and Germanium Nanowires. *J. Mater. Chem. C* **2013**, *1*, 4996–5007.

(19) Geaney, H.; Dickinson, C.; Barrett, C. A.; Ryan, K. M. High Density Germanium Nanowire Growth Directly from Copper Foil by Self-Induced Solid Seeding. *Chem. Mater.* **2011**, *23*, 4838–4843.

(20) Barth, S.; Koleśnik, M. M.; Donegan, K.; Krstić, V.; Holmes, J. D. Diameter-Controlled Solid-Phase Seeding of Germanium Nanowires: Structural Characterization and Electrical Transport Properties. *Chem. Mater.* **2011**, *23*, 3335–3340.

(21) Lensch-Falk, J. L.; Hemesath, E. R.; Lopez, F. J.; Lauhon, L. J. Vapor-Solid-Solid Synthesis of Ge Nanowires from Vapor-Phase-Deposited Manganese Germanide Seeds. *J. Am. Chem. Soc.* **2007**, *129*, 10670–10671.

(22) Tuan, H.-Y.; Lee, D. C.; Hanrath, T.; Korgel, B. A. Germanium Nanowire Synthesis: An Example of Solid-Phase Seeded Growth with Nickel Nanocrystals. *Chem. Mater.* **2005**, *17*, 5705–5711.

(23) Tuan, H.-Y.; Lee, D. C.; Hanrath, T.; Korgel, B. A. Catalytic Solid-Phase Seeding of Silicon Nanowires by Nickel Nanocrystals in Organic Solvents. *Nano Lett.* **2005**, *5*, 681–684.

(24) Mullane, E.; Geaney, H.; Ryan, K. M. Size Controlled Growth of Germanium Nanorods and Nanowires by Solution Pyrolysis Directly on a Substrate. *Chem. Commun.* **2012**, *48*, 5446–5448.

(25) Kang, K.; Gu, G. H.; Kim, D. A.; Park, C. G.; Jo, M.-H. Self-Organized Growth of Ge Nanowires from Ni-Cu Bulk Alloys. *Chem. Mater.* **2008**, *20*, 6577−6579.
(26) Kang, K.; Kim, D. A.; Lee, H.-S.; Kim, C.-J.; Yang, J.-E.; Jo, M.-H. Low-Temperature Deterministic Growth of Ge Nanowires Using Cu Solid Catalysts. *Adv. Mater.* **2008**, *20*, 4684−4690.
(27) Barrett, C. A.; Geaney, H.; Gunning, R. D.; Laffir, F. R.; Ryan, K. M. Perpendicular Growth of Catalyst-Free Germanium Nanowire Arrays. *Chem. Commun.* **2011**, *47*, 3843−3845.
(28) Geaney, H.; Dickinson, C.; Weng, W.; Kiely, C. J.; Barrett, C. A.; Gunning, R. D.; Ryan, K. M. Role of Defects and Growth Directions in the Formation of Periodically Twinned and Kinked Unseeded Germanium Nanowires. *Cryst. Growth Des.* **2011**, *11*, 3266−3272.
(29) Geaney, H.; Kennedy, T.; Dickinson, C.; Mullane, E.; Singh, A.; Laffir, F.; Ryan, K. M. High Density Growth of Indium Seeded Silicon Nanowires in the Vapor Phase of a High Boiling Point Solvent. *Chem. Mater.* **2012**, *24*, 2204−2210.
(30) Davidson, F. M.; Lee, D. C.; Fanfair, D. D.; Korgel, B. A. Lamellar Twinning in Semiconductor Nanowires. *J. Phys. Chem. C* **2007**, *111*, 2929−2935.
(31) Barth, S.; Boland, J. J.; Holmes, J. D. Defect Transfer from Nanoparticles to Nanowires. *Nano Lett.* **2011**, *11*, 1550−1555.
(32) Baggetto, L.; Notten, P. H. J. Lithium-ion (De) Insertion Reaction of Germanium Thin-Film Electrodes: An Electrochemical and In Situ XRD Study. *J. Electrochem. Soc.* **2009**, *156*, A169−A175.
(33) Baggetto, L.; Hensen, E. J.; Notten, P. H. In situ X-ray Absorption Spectroscopy of Germanium Evaporated Thin Film Electrodes. *Electrochim. Acta* **2010**, *55*, 7074−7079.
(34) Graetz, J.; Ahn, C.; Yazami, R.; Fultz, B. Nanocrystalline and Thin Film Germanium Electrodes with High Lithium Capacity and High Rate Capabilities. *J. Electrochem. Soc.* **2004**, *151*, A698−A702.
(35) Liu, X. H.; Huang, S.; Picraux, S. T.; Li, J.; Zhu, T.; Huang, J. Y. Reversible Nanopore Formation in Ge Nanowires During Lithiation-Delithiation Cycling: An In Situ Transmission Electron Microscopy Study. *Nano Lett.* **2011**, *11*, 3991−3997.